Quantum optomechanics in the bistable regime

R. Ghobadi,[1,2] A. R. Bahrampour,[2] and C. Simon[1]
[1]*Institute for Quantum Information Science and Department of Physics and Astronomy, University of Calgary, Calgary T2N 1N4, Alberta, Canada*
[2]*Department of Physics, Sharif University of Technology, Tehran, Iran*
(Received 20 April 2011; published 22 September 2011)

We study the simplest optomechanical system with a focus on the bistable regime. The covariance matrix formalism allows us to study both cooling and entanglement in a unified framework. We identify two key factors governing entanglement; namely, the bistability parameter (i.e., the distance from the end of a stable branch in the bistable regime) and the effective detuning, and we describe the optimum regime where entanglement is greatest. We also show that, in general, entanglement is a nonmonotonic function of optomechanical coupling. This is especially important in understanding the optomechanical entanglement of the second stable branch.

DOI: 10.1103/PhysRevA.84.033846 PACS number(s): 37.30.+i, 42.50.Pq, 42.50.Wk, 03.67.Bg

I. INTRODUCTION

Observing quantum effects like superposition states or entanglement at the macroscopic level is a long-standing goal. It is a widely held view that this should be possible, provided that environmentally induced decoherence can be sufficiently suppressed. Note, however, that there are some theoretical proposals which would rule out the existence of quantum effects at the macroscopic level (see e.g., Ref. [1]). Proposals for the experimental observation of macroscopic quantum effects are often based on the principle of Schrödinger's cat; that is, on coupling a microscopic quantum system to a macroscopic system in a controlled way in order to create a macroscopic superposition state [2–4].

One particularly promising approach in this context is the use of optomechanical systems. The most basic optomechanical system consists of a Fabry-Perot cavity with one movable end mirror. The position of this mirror is determined by the radiation pressure inside the cavity. Such systems were first studied in the context of high-precision measurements and gravitational wave detection [5]. It was suggested in Ref. [3] that the radiation pressure of a single photon in a high-finesse optical cavity could in principle create a macroscopic superposition of two spatially distinct locations of a movable mirror. A potential implementation of this idea was proposed in Ref. [4]. It is very challenging experimentally to achieve sufficiently strong optomechanical coupling at the single-photon level, requiring a system that combines high optical and mechanical finesse, a low mechanical resonance frequency, and ultralow temperature.

One way to enhance the optomechanical interaction is to pump the cavity with a strong laser. Using this technique the strong-coupling regime in optomechanical systems has recently been reached [6]. In the presence of a sufficiently strong driving laser the field enhancement inside the high-finesse optical cavity is large enough to trigger nonlinear behavior of the system. Depending on the input power and the detuning of the driving laser with respect to the cavity resonance, optomechanical systems exhibit different types of nonlinear behavior. For sufficiently strong input power, in the blue-detuned regime one obtains multistability [7], instability [8], and chaotic motion [9]. In the red-detuned regime bistability [10,11] occurs. Here we consider the red-detuned regime. This is the appropriate regime for cooling the mechanical oscillator close to the ground state [12,13], which is usually seen as a prerequisite for observing quantum effects. We are particularly interested in the relationship between bistability and entanglement.

Optomechanical bistability can be understood intuitively as the result of a competition between the mechanical restoring force, which increases linearly when the mirror is moved from its equilibrium position, and the radiation pressure force, which has a maximum at the cavity resonance. For a suitable set of parameters, as in Fig. 1, there are three intersection points between the two forces. The leftmost and rightmost intersection points correspond to stable states, because the restoring force grows faster than the radiation pressure (for the rightmost point the radiation pressure even decreases as the mirror is pushed outwards). In contrast, the middle intersection point is unstable because the radiation pressure force increases faster than the restoring force.

It is known that the optomechanical interaction can squeeze the cavity mode, and this squeezing becomes maximal close to the bistable regime [14]. It has also been noted [15] that, under certain conditions, entanglement is maximized at the bistability threshold. This was interpreted as being due to the enhanced optomechanical coupling strength in this region. Here, we analyze in detail entanglement close to and in the bistable regime. We show that a lot of insight can be gained by analyzing the situation in terms of two key parameters; namely, the effective detuning and the bistability parameter, which quantifies the distance from the end of each bistable branch. Cooling and entanglement can be studied in the same theoretical framework based on the covariance matrix. We identify the optimal regimes for both cooling and entanglement. We also show that, somewhat surprisingly, entanglement is in general a nonmonotonic function of the optomechanical coupling strength. (Naively, one might have expected it to always increase with optomechanical coupling strength.)

The paper is organized as follows: Section II introduces the optomechanical system and describes the linearization of the equations of motion around the steady state. We also show how bistability arises in the red-detuned regime in this framework, introduce the bistability parameter, and derive the dependence of the photon and phonon number on this parameter, which

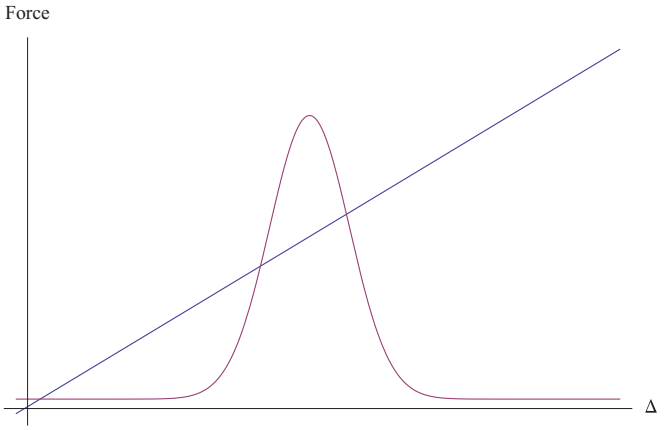

FIG. 1. (Color online) Mechanical restoring force and radiation pressure force around a cavity resonance. The leftmost and rightmost intersection points are stable equilibrium positions, whereas the middle one is unstable.

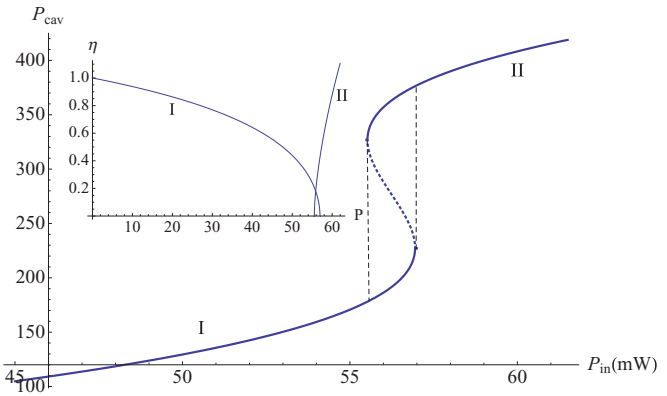

FIG. 2. (Color online) Bistability of the intracavity power with respect to input power. The solid and dotted lines correspond to the stable and unstable branches, respectively. The inset shows the bistability parameter η for the two stable branches. The end of each stable branch corresponds to $\eta = 0$.

leads us to a discussion of cooling. Section III discusses the optomechanical entanglement and its dependence on the bistability parameter and the effective detuning. This allows us to determine the optimum value for the detuning and the maximum achievable entanglement in our system. We discuss the role of the optomechanical coupling constant, show how entanglement varies on both stable branches in the bistable regime, and discuss its robustness under increasing temperature. Section IV is a summary and conclusion.

II. THE SYSTEM

We consider a high Q Fabry-Perot cavity with decay rate κ. The movable mirror can move under the influence of radiation pressure and thermal noise. The movable mirror is initially in equilibrium with a thermal bath at temperature T which results in the mechanical damping rate γ_m and the noise force $\xi(t)$. The system is driven by a laser with frequency ω_L and power P. The general Hamiltonian of such a system is derived in [16]. In the regime of parameters that we are interested in, the general Hamiltonian simplifies to [16,17]

$$H = \hbar\omega_c a^\dagger a + \frac{\hbar\omega_m}{2}(p^2+q^2) - \hbar G_0 a^\dagger a q + i\hbar E(a^\dagger e^{-i\omega_L t} - a e^{i\omega_L t}), \quad (1)$$

where ω_c and a are the frequency and the annihilation operator of the cavity mode, respectively, ω_m, q, and p are the frequency and the dimensionless position and momentum operators of the mirror, respectively, $G_0 = \frac{\omega_c}{L}\sqrt{\hbar/(m\omega_m)}$ is the coupling constant, and $E = \sqrt{2P\kappa/(\hbar\omega_L)}$ where P and ω_L are the input laser power and frequency, respectively. The first two terms correspond to two free harmonic oscillators, the third term corresponds to the optomechanical coupling, and the last term corresponds to the cavity being driven by the laser.

The equations of motion in the presence of damping and noise are

$$\dot{q} = \omega_m p, \quad (2)$$

$$\dot{p} = -\omega_m q - \gamma_m p + G_0 a^\dagger a + \xi(t), \quad (3)$$

$$\dot{a} = -(\kappa + i\Delta_0)a + iG_0 a q + E + \sqrt{2\kappa}a_{in}, \quad (4)$$

where $\Delta_0 = \omega_c - \omega_L$, a_{in} is the vacuum input noise of the cavity, and $\xi(t)$ is the noise associated with the damping of the mechanical oscillator. The nonlinear Eqs. (3) and (4) can be linearized by expanding the operators around their steady state values $O_i = O_{i,s} + \delta O_i$, where $O_i = a, q, p$.

From Eqs. (2)–(4), the steady state solutions are $\alpha_s = E/[\kappa + i(\Delta_0 - G_0 q_s)]$, $q_s = G_0|\alpha_s|^2/\omega_m$, and $p_s = 0$, where α_s, q_s, and p_s are the stationary values for cavity amplitude, position, and momentum of the mechanical oscillator, respectively. Note that the last of these relations is a third-order polynomial equation for α_s, which has three roots. The largest and the smallest roots are stable, and the middle one is unstable. Figure 2 shows the hysteresis loop for the intracavity power. Consider P_{cav} initially on the lower stable branch (I in Fig. 2, corresponding to the smallest root). As P_{in} increases, P_{cav} approaches the end of that branch. At this point a little increase in the input power results in a switch of P_{cav} to the second stable branch (II in Fig. 2, corresponding to the largest root). If P_{in} is increased further, the system remains on the upper branch. If P_{in} is decreased, the system approaches the beginning of the second stable branch. If P_{in} is decreased even further, the system switches back to the lower stable branch. We have used the set of parameters of Ref. [17], which is close to several optomechanical experiments [18–21]. We consider a Fabry-Perot cavity with length $L = 1$ mm and finesse $\mathcal{F} = 1.07 \times 10^4$, driven by a laser with $\lambda = 810$ nm and $\Delta_0 = 2.62\omega_m$. The mechanical oscillator frequency, damping rate, and mass are 10 MHz, 100 Hz, and 5 ng, respectively, with an environment temperature $T = 400$ mK.

By introducing $u^T(t) = (\delta q(t), \delta p(t), X(t), Y(t))$ and $n^T(t) = (0, \xi(t), \sqrt{2\kappa}X_{in}(t), \sqrt{2\kappa}Y_{in}(t))$, where $X = (\delta a + \delta a^\dagger)/\sqrt{2}$ and $Y = (\delta a - \delta a^\dagger)/(\sqrt{2}i)$, and corresponding noises X_{in} and Y_{in}, the linearized dynamics of system can be written in a compact form

$$\dot{u}(t) = Au(t) + n(t), \quad (5)$$

where

$$A = \begin{pmatrix} 0 & \omega_m & 0 & 0 \\ -\omega_m & -\gamma_m & G & 0 \\ 0 & 0 & -\kappa & \Delta \\ G & 0 & -\Delta & -\kappa \end{pmatrix}, \tag{6}$$

and $G = \sqrt{2}G_0\alpha_s$ and $\Delta = \Delta_0 - G_0 q_s$ are the enhanced optomechanical coupling rate and effective detuning, respectively.

Since the initial state of the system is Gaussian and the dynamical equations are linear in the creation and annihilation operators both for the cavity and mechanical mode, the state of the system remains Gaussian at all times. A Gaussian state is fully characterized by its covariance matrix which is defined at any given time t by $V_{ij}(t) = \frac{1}{2}\langle u_i(t)u_j(t) + u_j(t)u_i(t)\rangle$. The mechanical and optical input-noise operators are fully characterized by their correlation function, which in the Markovian approximation are given by

$$\langle a_{\rm in}(t)a_{\rm in}^{\dagger}(t')\rangle = \delta(t-t'), \tag{7}$$

$$\frac{\langle \xi(t)\xi(t') + \xi(t')\xi(t)\rangle}{2} = \gamma_m(2\bar{n}+1)\delta(t-t'), \tag{8}$$

where $\bar{n} = [\exp(\frac{\hbar\omega_m}{k_B T}) - 1]^{-1}$ is the mean thermal phonon number and k_B is Boltzmann's constant. From Eqs. (5), (7), and (8), one obtains the equation of motion for the covariance matrix, which is given by [22]

$$\dot{V} = AV + VA^T + D. \tag{9}$$

The steady state solution for the covariance matrix ($\dot{V} = 0$) is reached if all the eigenvalues of the matrix A have negative real parts. In the red-detuned regime of operation ($\Delta > 0$), the Routh-Hurwitz criterion [23] gives the following stability condition:

$$\omega_m(\kappa^2 + \Delta^2) - G^2\Delta > 0. \tag{10}$$

In the following we use the dimensionless "bistability parameter" defined as [24]

$$\eta = 1 - \frac{G^2\Delta}{\omega_m(\kappa^2+\Delta^2)}, \tag{11}$$

which is a positive number between zero and one, according to Eq. (10), in the red-detuned regime ($\Delta > 0$). We have shown the bistability parameter in the inset of Fig. 2. As can be seen from Fig. 2, η decreases when approaching the bistable regime and becomes equal to zero at the end of each stable branch.

Equation (10) can be intuitively understood by ignoring retardation effects for the radiation pressure. Assuming that the optical field adiabatically follows the mechanical oscillator (i.e., setting $\dot{\delta a} = 0$), one has $\delta a = (\frac{1}{\sqrt{2}} iG\delta q + \sqrt{2\kappa}a_{\rm in})/(\kappa + i\Delta)$. The equation of motion for the mirror becomes

$$\dot{\delta p} = -\left(\omega_m - \frac{G^2\Delta}{\kappa^2+\Delta^2}\right)\delta q - \gamma_m \delta p + \xi_T, \tag{12}$$

where $\xi_T = \xi + G\sqrt{2\kappa}[a_{\rm in}/(\kappa + i\Delta) + a_{\rm in}^{\dagger}/(\kappa - i\Delta)]$. From Eq. (11), we see that the mechanical oscillator is stable if the first coefficient is positive. In this case the first term in Eq. (12) corresponds to a harmonic restoring force; see also Fig. 1 and the associated discussion. This implies the stability condition (10). The adiabatic approximation is equivalent to treating the response of the cavity field to the moving mirror as instantaneous. It is well known that the delayed nature of this response gives rise to cooling [25], which is, however, not essential for the above argument. We feel that this argument helps the physical understanding of the stability condition. However, let us emphasize that we do not make the adiabatic approximation in what follows.

In the bistable regime, the fluctuations around the steady state solution diverge as one approaches the end of each stable branch. To show this explicitly we solve Eq. (9) for the steady state, from which we can obtain the phonon and photon numbers by using $\bar{n}_m = \frac{1}{2}(V_{11} + V_{22} - 1)$ and $\bar{n}_o = \frac{1}{2}(V_{33} + V_{44} - 1)$. The general solution is complicated and not very illuminating. Simple relations that show the dependence of the fluctuations on the stability parameter can be obtained by assuming a high mechanical quality factor and a low-temperature environment [i.e., $\omega_m/\gamma_m \ll 1$ and $\kappa/(\bar{n}\gamma_m) \gg 1$]. We find

$$\bar{n}_m = \frac{(\Delta^2+\kappa^2)(1+\eta) - 2\eta\omega_m(2\Delta - \omega_m)}{8\Delta\eta\omega_m}, \tag{13}$$

$$\bar{n}_o = \frac{(1-\eta)(\kappa^2+\Delta^2)}{8\eta\Delta^2}. \tag{14}$$

From Eqs. (13) and (14) it is clear that the phonon and photon numbers diverge as η approaches zero. In order to stay within the range of validity of the linearization approximation, we have made sure that $\bar{n}_o \ll |\alpha_s|^2$ in all the results shown below.

For $\eta \sim 1$ from Eq. (13) the optimum value for the detuning which minimizes the phonon number is given by

$$\Delta_{\rm opt} = \sqrt{\kappa^2 + \omega_m^2}. \tag{15}$$

Using the optimum value for detuning in Eq. (13), one finds

$$\bar{n}_m = \frac{1}{2}\left(\frac{\sqrt{\kappa^2+\omega_m^2}}{\omega_m} - 1\right), \tag{16}$$

which is identical to Eq. (7) in [26]. In the resolved sideband regime ($\omega_m \gg \kappa$) one sees from Eq. (15) that ground-state cooling can be achieved [$\bar{n}_m = \kappa^2/(4\omega_m^2)$] [26,27].

III. OPTOMECHANICAL ENTANGLEMENT

As shown in [28], for bipartite Gaussian states the Peres-Horodecki criterion [29,30] (positivity of the density matrix under partial transposition) is necessary and sufficient for separability. In terms of the covariance matrix formalism this criterion is called logarithmic negativity, which is defined as [31]

$$E_N = \max\{0, -\ln(2\nu_{\rm min})\}, \tag{17}$$

where $\nu_{\rm min}$ is the smallest symplectic eigenvalue of the partially transposed covariance matrix given by $\nu_{\rm min} = [\frac{1}{2}(\Sigma - \sqrt{\Sigma^2 - 4\det V})]^{1/2}$, where $\Sigma = \det A + \det B - 2\det C$ and we represent the covariance matrix in terms of

$$V = \begin{pmatrix} A & C \\ C^T & B \end{pmatrix}. \tag{18}$$

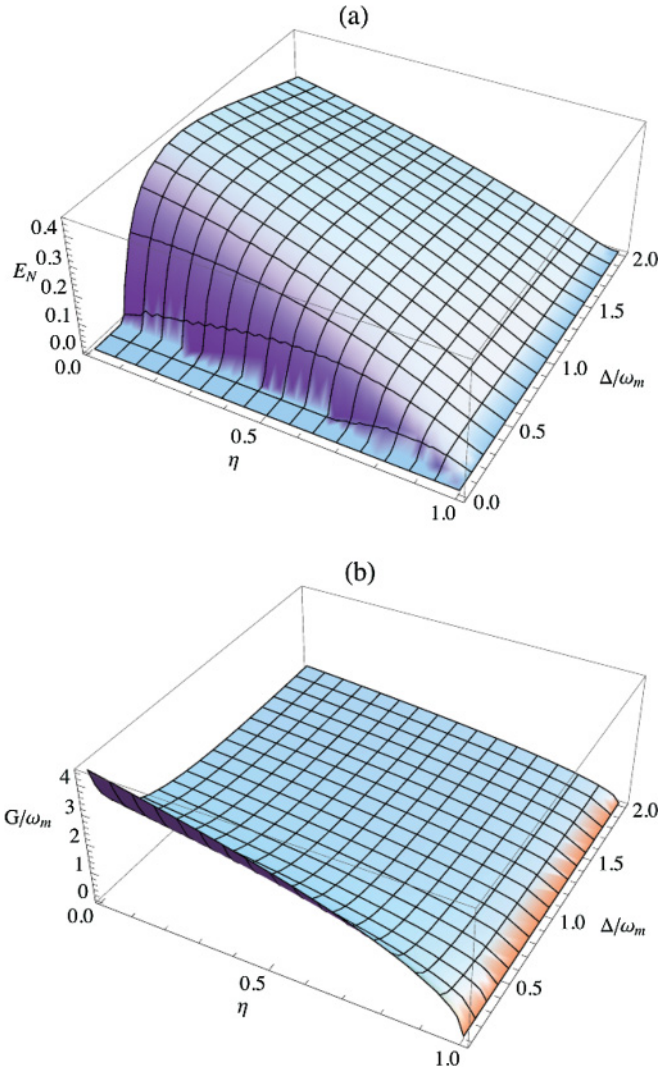

FIG. 3. (Color online) Optomechanical entanglement (a) and optomechanical coupling constant (b) as a function of bistability parameter η and normalized effective detuning Δ/ω_m for a cavity decay rate $\kappa = 1.4\omega_m$.

Equipped with this measure we go on to study optomechanical entanglement. Figure 3(a) shows the logarithmic negativity as a function of bistability parameter η and effective detuning Δ. We note that, for $\eta \sim 1$, which is required for ground-state cooling, there is no optomechanical entanglement. From Fig. 3(a) one can identify three different regimes depending on the effective detuning. In the first regime, for the smallest detuning, there is no optomechanical entanglement. In the second regime, for intermediate values of the detuning, there is some optomechanical entanglement, but the maximum value for entanglement is attained for values of the bistability parameter η somewhere between zero and one. This means that, for these values of the detuning, the maximum entanglement does not occur at the end of the bistable branch (cf. [15]). Finally, in the third regime, for the largest values of detuning, there is strong optomechanical entanglement and, for each fixed value of detuning, the maximum entanglement is in fact reached at the end of the branch (i.e., for $\eta = 0$).

Figure 3(b) shows the corresponding optomechanical coupling in the different regimes. From Fig. 3(b) it is clear that optomechanical coupling is a monotonically decreasing function of effective detuning (i.e., $G_1 > G_2 > G_3$ where G_i is the optomechanical coupling constant in the ith regime). So we see that, in general, entanglement is not a monotonically increasing function of the coupling constant. These observations suggest that the key variables that determine the entanglement behavior are the effective detuning and the bistability parameter, not the optomechanical coupling constant.

A more quantitative understanding of the different regimes for entanglement is possible by looking at the entanglement behavior in the vicinity of $\eta = 0$. Assuming that $\omega_m/\gamma_m \gg 1$ and $\kappa/(\bar{n}\gamma_m) \gg 1$, one finds $\Sigma = a + b/\eta$ and $\det V = c + d/\eta$, where

$$a = \frac{\Delta^2 - 3\kappa^2 + \omega_m^2}{16\Delta^2}, \tag{19}$$

$$b = \frac{(\Delta^2 + \kappa^2)\left(\Delta^2 + \kappa^2 + 5\omega_m^2\right)}{16\Delta^2\omega_m^2}, \tag{20}$$

$$c = \frac{2\Delta^2(\Delta^2 + \kappa^2) + (\Delta^2 - \kappa^2)\omega_m^2}{128\Delta^4}, \tag{21}$$

$$d = \frac{(\Delta^2 + \kappa^2)\left(4\Delta^4 + 4\Delta^2\kappa^2 + 4\Delta^2\omega_m^2 + \omega_m^4\right)}{256\Delta^4\omega_m^2}. \tag{22}$$

From these equations it is possible to derive a simple form for the logarithmic negativity. Close to the bistability region ($\eta \ll 1$) we have $E_N = \max\{0, \alpha + \beta\eta\}$, where $\alpha = -\ln(2\sqrt{d/b})$ and $\beta = (abd - b^2c - d^2)/(2db^2)$.

It is worth noting that, in contrast to the phonon and photon numbers, which diverge for $\eta = 0$, the logarithmic negativity has a finite limiting value given by α. While our linearization approximation is not justified for the point $\eta = 0$ itself, it does apply in its close vicinity, as the photon number drops precipitously as one moves away from the endpoint of the stable branch [cf. Eq. (14)].

Using our expression for entanglement close to bistability one can easily identify the three regimes shown in Fig. 3. Figure 4 shows the plot for α and β. From Fig. 4 one can identify the boundaries between the different regimes discussed above. The first regime corresponds to $\alpha < 0$ or, equivalently, $\Delta < 0.25\omega_m$. The second regime corresponds to

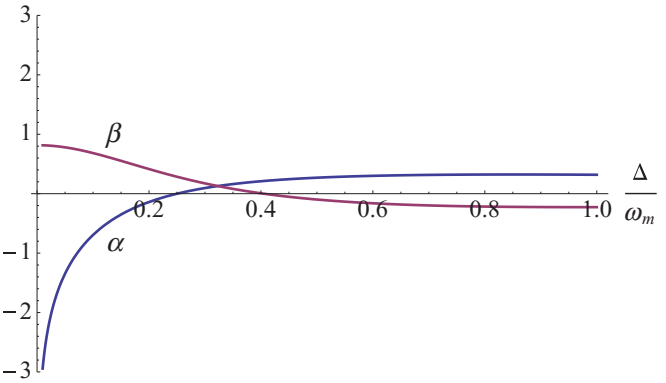

FIG. 4. (Color online) Plot of α and β as a function of normalized detuning. The parameters are the same as in Fig. 3.

$\alpha > 0$ and $\beta > 0$ or $0.25\omega_m < \Delta < 0.4\omega_m$. Finally, the third regime corresponds to $\alpha > 0$ and $\beta < 0$ or $\Delta > 0.4\omega_m$.

Moreover, as can be seen from Fig. 3, the maximum optomechanical entanglement is reached in the bistability region (for η approaching 0) in the third regime. So the maximum achievable optomechanical entanglement is given by α. From Eqs. (19)–(22) the optimum value for effective detuning where entanglement takes its maximum value is

$$\Delta_{\rm opt} = \frac{\omega_m}{4}\sqrt{1+\sqrt{16\left(\frac{\kappa}{\omega_m}\right)^2+81}}. \tag{23}$$

For $\kappa = 1.4\omega_m$, we obtain from Eq. (23) $\Delta_{\rm opt} = 0.85\omega_m$. Comparing this to Eq. (15) one sees that the optimum effective detuning values for cooling and entanglement are not the same. Even more importantly, the cooling performance is optimized for $\eta = 1$, whereas entanglement becomes maximal for $\eta = 0$. Using the optimum value for detuning we obtain the following expression for the maximum achievable entanglement in our system:

$$E_{N,\max} = -\ln\left[\frac{1}{5}\sqrt{9+\frac{128\kappa^2}{8\kappa^2+45\omega_m^2}}\right]. \tag{24}$$

Note that this takes its greatest possible value for $\kappa \ll \omega_m$, giving $E_{N,\max} = -\ln(3/5) = 0.51$.

It is also interesting to look at the optomechanical entanglement for the two stable branches and their behavior in the bistable regime. Figure 5 shows the logarithmic negativity as a function of input power for both stable branches. Varying the input power corresponds to varying η (cf. Fig. 2). We note the persistence of entanglement in the second stable state in a very narrow window of parameter space. As can be seen in Fig. 5, the entanglement is maximum at the end of each branch, corresponding to the third regime. The fast decreasing entanglement for the second branch is in agreement with the bistability parameter behavior in Fig. 2. The inset to Fig. 5 shows the optomechanical coupling for different stable branches. One sees clearly that the coupling constant is not the decisive parameter for the amount of entanglement

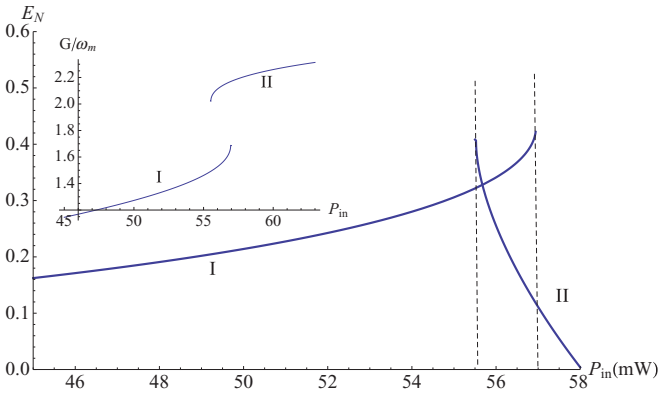

FIG. 5. (Color online) Plot of optomechanical entanglement as a function of input power for both stable branches. The dot dashed (dashed) line corresponds to the end of the first (second) stable branch. The parameters are the same as in Fig. 2.

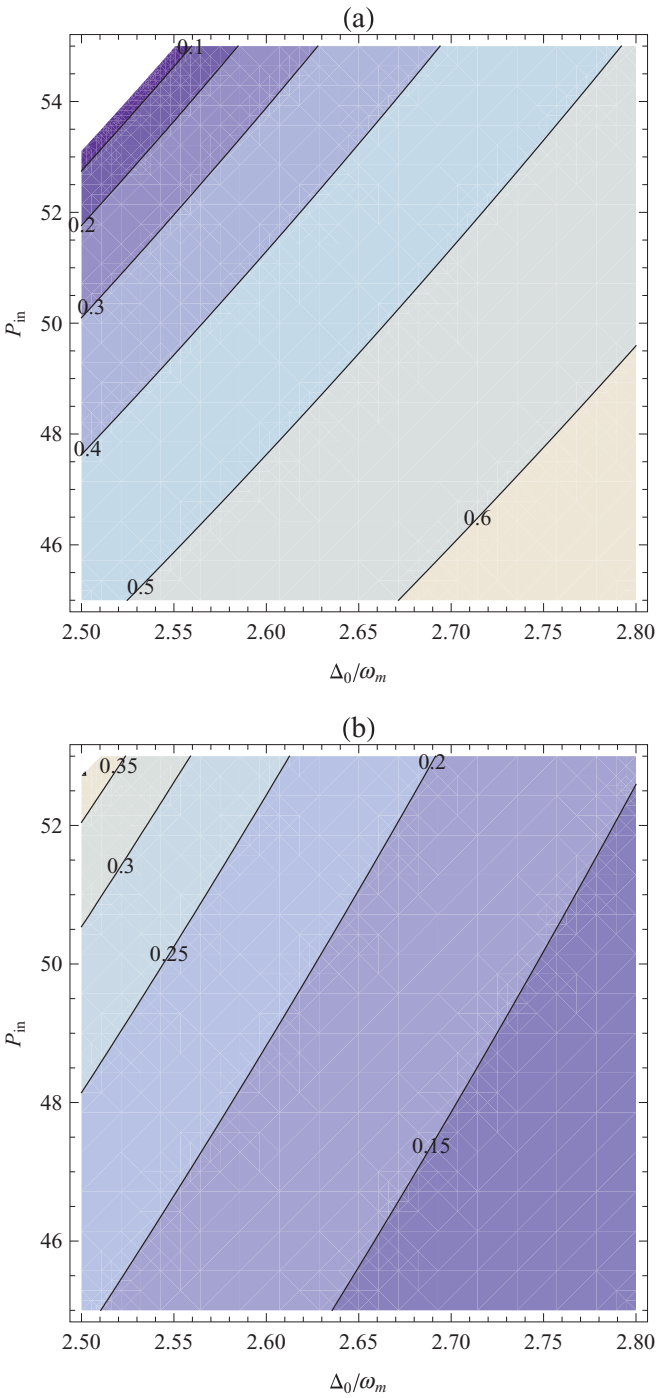

FIG. 6. (Color online) Contour plot for bistability parameter (a) and entanglement (b) versus bare detuning Δ_0 and input power $P_{\rm in}$ in mW. The parameters are the same as in Fig. 2.

in our system and, in particular, that the entanglement is a nonmonotonic function of the coupling constant.

Until now we studied the entanglement in terms of parameters that are natural to use from a theoretical point of view. It is also interesting to look at entanglement in terms of parameters that can be directly controlled experimentally. Figure 6 shows the bistability parameter and entanglement as a function of bare detuning Δ_0 and laser power P. Note that, as we come

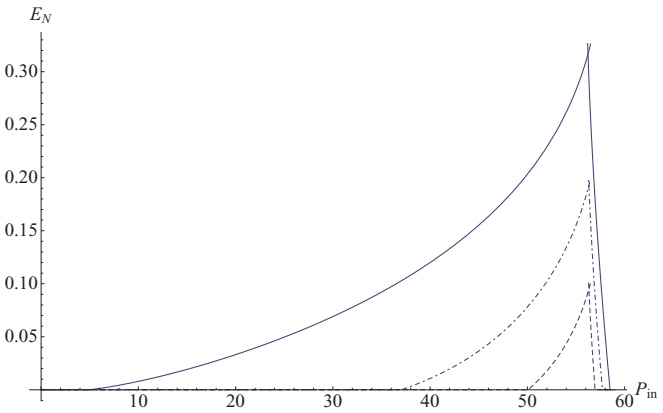

FIG. 7. (Color online) Plot of logarithmic negativity versus input power (mW) for different environment temperatures: $T = 0.4$ K (solid line), $T = 5$ K (dot dashed), and $T = 10$ K (dashed). The other parameters are the same as in Fig. 2.

close to the end of the branch for suitable detuning and for sufficiently large input power, the entanglement increases.

We have also studied the robustness of entanglement with respect to the temperature. The result is shown in Fig. 7. One sees that, for higher temperatures, the entanglement survives only in the vicinity of the bistable region.

Finally, we note that, in the recent experiment [32], the ratio of the input power to the critical power (i.e., the input power for which the bistability happens) is about 0.5. So the bistable regime should definitely be accessible experimentally.

IV. CONCLUSION

We have studied the simplest optomechanical system using the covariance matrix formalism with a special emphasis upon bistability. We recovered the standard results upon optomechanical cooling as a special case of our general expression for the phonon number. However, our focus was on entanglement. We identified two key parameters; namely, the effective detuning and the bistability parameter (i.e., the distance from the end of each stable branch in the bistable regime), and we showed that there are different regimes for entanglement as a function of these parameters. In particular, we showed that maximum entanglement is achieved when the system is simultaneously close to the red sideband (in terms of effective detuning) and close to the end of each stable branch (bistability parameter close to zero). We also showed that the dependence of entanglement on the optomechanical coupling is counter intuitive and that, in the bistable regime, the entanglement is particularly robust with respect to temperature increases.

It would be very interesting to see experimental explorations of the phenomena described in the present paper. However, it should be noted that measuring the covariance matrix, which lies at the heart of our analysis, requires direct access to the position and momentum variables of the mirror, not just the quadratures of the light. It seems that this would require either an auxiliary measurement cavity, as proposed in Ref. [17], or at least an additional laser beam. A detailed analysis of the resulting more complex dynamics is work for the future. In the present paper we focused on the entanglement characteristics of the basic system, which are already quite rich and intriguing.

ACKNOWLEDGMENTS

We thank D. Bouwmeester, A. D'Souza, D. Kleckner, A. Lvovsky, and B. Pepper for very useful discussions. This work was supported by AITF and NSERC.

[1] R. Penrose, in *Mathematical Physics 2000*, edited by A. Fokas *et al.* (Imperial College, London, 2000).
[2] A. D. Armour, M. P. Blencowe, and K. C. Schwab, Phys. Rev. Lett. **88**, 148301 (2002).
[3] S. Bose, K. Jacobs, and P. L. Knight, Phys. Rev. A **59**, 3204 (1999).
[4] W. Marshall, C. Simon, R. Penrose, and D. Bouwmeester, Phys. Rev. Lett. **91**, 130401 (2003).
[5] V. B. Braginsky, *Measurement of Weak Forces in Physics Experiments* (University of Chicago Press, Chicago, 1977).
[6] S. Groblacher, K. Hammerer, M. R. Vanner, and M. Aspelmeyer, Nature (London) **460**, 724 (2009).
[7] F. Marquardt, J. G. E. Harris, and S. M. Girvin, Phys. Rev. Lett. **96**, 103901 (2006).
[8] O. Arcizet, P.-F. Cohadon, T. Briant, M. Pinard, and A. Heidmann, Nature (London) **444**, 71 (2006).
[9] T. Carmon, M. C. Cross, and Kerry J. Vahala, Phys. Rev. Lett. **98**, 167203 (2007).
[10] A. Dorsel, J. D. McCullen, P. Meystre, E. Vignes, and H. Walther, Phys. Rev. Lett. **51**, 1550 (1983).
[11] M. Karuza, C. Biancofiore, M. Galassi, R. Natali, G. Di Giuseppe, P. Tombesi, D. Vitali, e-print arXiv:1012.5632.
[12] R. Riviere, S. Deleglise, S. Weis, E. Gavartin, O. Arcizet, A. Schliesser, and T. J. Kippenberg, Phys. Rev. A **83**, 063835 (2011).
[13] J. D. Teufel, T. Donner, Dale Li, J. H. Harlow, M. S. Allman, K. Cicak, A. J. Sirois, J. D. Whittaker, K. W. Lehnert, and R. W. Simmonds, Nature **475**, 359 (2011).
[14] C. Fabre, M. Pinard, S. Bourzeix, A. Heidmann, E. Giacobino, and S. Reynaud, Phys. Rev. A **49**, 1337 (1994).
[15] C. Genes, A. Mari, P. Tombesi, and D. Vitali, Phys. Rev. A **78**, 032316 (2008).
[16] C. K. Law, Phys. Rev. A **51**, 2537 (1995).
[17] D. Vitali, S. Gigan, A. Ferreira, H. R. Bohm, P. Tombesi, A. Guerreiro, V. Vedral, A. Zeilinger, and M. Aspelmeyer, Phys. Rev. Lett. **98**, 030405 (2007).
[18] D. Kleckner, W. Marshall, M. J. A. deDood, K. N. Dinyari, B. J. Pors, W. T. M. Irvine, and D. Bouwmeester, Nature (London) **444**, 75 (2006).

[19] S. Gigan, H. R. Bohm, M. Paternostro, F. Blaser, G. Langer, J. B. Hertzberg, K. C. Schwab, D. Bauerle, M. Aspelmeyer, and A. Zeilinger, Nature (London) **444**, 67 (2006).
[20] D. Kleckner, W. Marshall, M. J. A. deDood, K. N. Dinyari, B. J. Pors, W. T. M. Irvine, and D. Bouwmeester, Phys. Rev. Lett. **96**, 173901 (2006).
[21] T. Carmon, H. Rokhsari, L. Yang, T. J. Kippenberg, and K. J. Vahala, Phys. Rev. Lett. **94**, 223902 (2005).
[22] A. Mari and J. Eisert, Phys. Rev. Lett. **103**, 213603 (2009).
[23] E. X. DeJesus and C. Kaufman, Phys. Rev. A **35**, 5288 (1987).
[24] C. Genes, D. Vitali, P. Tombesi, S. Gigan, and M. Aspelmeyer, Phys. Rev. A **77**, 033804 (2008).
[25] C. Hohberger Metzger and K. Karrai, Nature (London) **432**, 1002 (2004).
[26] I. Wilson-Rae, N. Nooshi, W. Zwerger, and T. J. Kippenberg, Phys. Rev. Lett. **99**, 093901 (2007).
[27] F. Marquardt, J. P. Chen, A. A. Clerk, and S. M. Girvin, Phys. Rev. Lett. **99**, 093902 (2007).
[28] R. Simon, Phys. Rev. Lett. **84**, 2726 (2000).
[29] A. Peres, Phys. Rev. Lett. **77**, 1413 (1996).
[30] P. Horodecki, Phys. Lett. A **232**, 333 (1997).
[31] G. Adesso, A. Serafini, and F. Illuminati, Phys. Rev. A **70**, 022318 (2004).
[32] S. Groblacher, J. B. Hertzberg, M. R. Vanner, G. D. Cole, S. Gigan, K. C. Schwab, and M. Aspelmeyer, Nature Phys. **5**, 485 (2009).